THE ASTROPHYSICAL JOURNAL, 291:571–580, 1985 April 15

INFRARED SOURCES AND EXCITATION OF THE W40 COMPLEX

J. SMITH, A. BENTLEY, M. CASTELAZ, R. D. GEHRZ, G. L. GRASDALEN, AND J. A. HACKWELL
Wyoming Infrared Observatory, Department of Physics and Astronomy, University of Wyoming
Received 1984 August 8; accepted 1984 October 10

ABSTRACT

Infrared images and photometry are presented for the W40 molecular cloud and H II region complex. The images, sampled through a 5″ aperture and observed at effective wavelengths of 2.3, 3.6, 4.9, 10.0, and 19.5 μm, reveal only unresolved sources clustered near the peak of thermal H II emission. Six of the seven detected sources coincide with faint but optically observable stars. The photometry suggests that the three brightest sources are heavily obscured early-type stars surrounded by infrared emitting circumstellar materials. In some cases, much of the compact infrared emission may be produced by circumstellar condensations.

The three brightest sources (IRS 1a, 2a, and 3a) are candidates for producing the level of excitation inferred for both the dust and H II plasma of the W40 complex. Observed circumstellar dust has a negligible effect on the excitation of the W40 region. Instead, the predominant mode of excitation, whereby radiant luminosities of the exciting stars are absorbed by the W40 dust, appears to involve only diffuse dust mixed with the molecules, atoms and plasma.

Subject headings: infrared: sources — interstellar: matter — nebulae: H II regions — nebulae: individual

I. INTRODUCTION

W40 is an H II region and molecular cloud complex lying 3°.5 above the galactic plane and approximately 700 pc from Earth. The H II region has a diameter of ~5′ and a moderate emission measure of ~1×10^5 pc cm^{-6} (Goss and Shaver 1970), showing that it has undergone the rapid phases of dynamical evolution normally associated with the formation and expansion of a compact H II region. Other components of the W40 complex are a 10′ × 20′ molecular cloud of moderate CO brightness temperature (Zeilik and Lada 1978), clouds of obscuring dust that radiate bright far-infrared and middle-infrared continua (Olthof 1974; Price and Walker 1976), and a cluster of infrared sources centered on the H II region (Zeilik and Lada 1978). Formed from these components, the W40 morphology can be described as an extensive molecular complex, the bright core of which lies in a side-by-side relationship with an evolved H II region and its sources of excitation.

In view of its distance from Earth, galactic environment, and observed morphology, the W40 complex should prove interesting for a variety of detailed studies pertinent to young stars and how they interact with their interstellar environments. For this study, we chose to concentrate on a small, ~3 arcmin^2 region centered near the position of peak H II emission. Our objective was to produce a detailed infrared study of the exciting sources of the H II region.

II. OBSERVATIONS

All measurements were made from the Wyoming Infrared Observatory (WIRO). The first step in data acquisition involved taking 64″ × 64″ images centered on the three bright 2.2 μm sources discovered and named IRS 1, 2, and 3 by Zeilik and Lada (1978). Each of the images was obtained using the methods described in Hackwell, Grasdalen, and Gehrz (1982) and Gehrz *et al.* (1982). For all of the observed images, including those required for the calibration stars, the sampling interval was 1″ with the reference aperture positioned 60″ north of the signal aperture. The aperture diameter was ~5″ (FWHM).

Thermal infrared emission produced by the telescope and sky must be removed from the total signal. For the $\lambda \geq 3.6$ μm images, which were observed with a bolometer detector, this terrestrial emission was corrected with a two-step process. First, reference aperture signals were subtracted from the image signals during data acquisition at the WIRO. Later, final reduction involved removing from each image any effects of spatial gradients in detected terrestrial emission. These effects were inferred from columns of pixels forming image boundaries, along which zero celestial emission was assumed.

Unlike the $\lambda \geq 3.6$ μm images observed with the bolometer AC coupled to its preamplifier, the 2.3 μm images were observed with a photovoltaic detector coupled directly in the current integrating mode to its preamplifier and data acquisition electronics. Since reference aperture signals were not subtracted, each pixel of integrated charge represents an absolute surface brightness. Each 2.3 μm surface brightness was corrected for terrestrial emission in much the same way described above for the $\lambda \geq 3.6$ μm images.

Guided by the preliminary imaging results, we began measuring optical-infrared energy distributions of the brightest imaged sources. Infrared photometry was done with reference aperture spacings ranging from 10″ to 60″. For the *UBV* photometry, the sky readings were taken 20″ north of each measured star. Apertures (FWHM) were 5″ for the 4.9 μm, mostly 5″ but occasionally 10″ for the *KL*, 10″ for the *JH*, and 12″ for the *UBV* photometry.

We calibrated the observed 4.9 μm flux densities and also most of the 2.3 and 3.6 μm flux densities with observations of the stars μ UMa, α Lyr, β Peg, and α Boo (Gehrz, Hackwell, and Jones 1974). See Johnson *et al.* (1966) for the flux densities of σ Her and ν Cyg, observations of which calibrated the *JH* and also the remaining *K* (2.3 μm) and *L* (3.6 μm) photometry.

Positions of the infrared sources were measured by peaking up on the individual sources and recording the telescope position. Observations of the IRC +00 360, SAO 142364, and SAO 142368 positions calibrated the W40 positions (Table 1), each measured with a ±1″ uncertainty.

TABLE 1

PARAMETERS OF THE INFRARED IMAGES OF FIGURE 1

$\lambda(\mu m)$	Maximum Level (Jy arcsec^{-2})	Faintest Level (mJy arcsec^{-2})	(percent)	([a]mag aperture^{-1})
2.3.........	0.17	2.6	1.5	10.5
3.6.........	0.26	16	6	7.6
4.9.........	0.26	31	12	5.8
10...........	1.9	56	3	3.8
19.5.........	4.1	520	12	−0.2

[a] FWHM ≈ 5″, and area ≈ 20 arcsec^2 for the aperture.

III. RESULTS

Figure 1 shows the five infrared images observed for portions of the W40 complex. Dashed lines give boundaries of the observed images ranging in size from 5 arcmin^2 for 2.3 μm down to 1 arcmin^2 for 4.9 and 19.5 μm. See the upper left corner of Figure 1*g* for representative point source responses for the photometers used to measure the images. Each response has ~20 arsec^2 for its integrated area and FWHM ≈ 5″. For each image, Table 1 gives the surface brightnesses corresponding to the maximum contour level of 100% and to the faintest level that was chosen to have the 3 σ statistical significance. The faintest levels are given in units of mJy arcsec^{-2}, percent of maximum surface brightness, and also magnitude per 5″ aperture.

The 2.3 μm image (Fig. 1*a*) consists of seven sources (IRS 1a, 1b, 1c, 1d, 2a, 2b, and 3a) clustered near the position of peak H II emission labeled by "H II" in Figure 1*g*. For $\lambda \geq 2.3$ μm (Figs. 1*a*–1*e*), each detected source has FWHM ≈ 5″, the size expected for a point source observed with our photometers; we find no significant evidence for extended emission at any observed wavelength. The positions of the infrared sources are given in Table 2. The positions of IRS 1a, 2a, and 3a agree with the positions given by Zeilik and Lada (1978) for IRS 1, 2, and 3.

A comparison of the 2.3 μm image with the POSS E print (Fig. 1*f*) shows that all but one (IRS 1b) of the seven infrared sources has an optical counterpart. Any optical counterpart to IRS 1b must have $R \gtrsim 20$, the limiting magnitude of the E print. Figure 1*g* and Table 2 give the positions and names of the optical sources. Two of the compact optical sources in Table 2, OS 2c and 4a, are visible in Figure 1*f*, but we did not detect infrared counterparts. Only OS 1a, 2a, and 3a are visible on the blue POSS print.

Of the infrared observations presented in Figure 1, the 2.3 μm image has the greatest sensitivity to main-sequence stars obscured by moderate column densities of dust. The 10.5 mag limit corresponds to the 2.3 μm mag of an unobscured B5 ZAMS star located at the W40 distance of 700 pc (see below). Therefore, any main-sequence stars too faint to appear in the 2.3 μm image should contribute negligibly to the O9 V level of H II excitation inferred below for W40.

The mean surface brightness of H II continuum emission extrapolated from the radio continuum measurements of W40 (Goss and Shaver 1970, beam = 4′; Zeilik and Lada 1978, beam = 2′) is approximately 20 times smaller than the limiting 3 σ surface brightness at 2.3 μm of $\sim 2 \times 10^{-3}$ Jy arcsec^{-2}. That limit and also the small 60″ reference aperture spacing explain why Figure 1*a* shows no diffuse H II emission.

The 2.2 μm map made by Zeilik and Lada (1978) with large sizes of aperture diameter (44″) and reference aperture spacing (240″) covers approximately the same region shown in Figure 1*a*. Summing the 2.3 μm flux densities of all seven infrared sources of Figure 1*a* gives 7.1 Jy, which approximates closely the 10 ± 1 Jy (corrected slightly from 2.2 to 2.3 μm) given by Zeilik and Lada for their map. This means that any diffuse emission detected by Zeilik and Lada must contribute less than ~3 Jy to the total 2.3 μm flux density of W40. The fact that the contour map presented by Zeilik and Lada appears to be a low resolution version of Figure 1*a* provides further support for the view that emission from compact infrared sources is larger than diffuse 2 μm emission from H II gas or hot dust in W40.

Table 3 gives the photometry plotted in Figure 2 for IRS 1a, 1b, 1c, 2a, and 3a. Entries in Table 3 are in magnitudes. Except where noted in Table 3, 1 σ uncertainties are ±0.1 mag.

TABLE 2

W40 POSITIONS

Names	α (1950)	δ (1950)
A. Compact Sources		
IRS 1a	18ʰ28ᵐ51ˢ.7	−2°07′34″
OS 1a	18 28 51.6	−2 07 35
IRS 1b	18 28 52.6	−2 07 42
IRS 1c	18 28 49.9	−2 07 28
OS 1c	18 28 49.7	−2 07 29
IRS 1d	18 28 51.4	−2 07 23
OS 1d	18 28 51.4	−2 07 22
IRS 2a	18 28 47.8	−2 07 41
OS 2a	18 28 47.5	−2 07 40
IRS 2b	18 28 46.5	−2 07 45
OS 2b	18 28 46.1	−2 07 43
OS 2c	18 28 49.0	−2 07 21
IRS 3a	18 28 47.8	−2 06 21
OS 3a	18 28 47.8	−2 06 22
OS 4a	18 28 50.3	−2 06 42
B. Large-Scale Sources		
H II	18 28 49.0	−2 07 35
CO-Peak 1	18 28 39.7	−2 08 58
CO-Peak 2	18 28 39	−2 04 25
AFGL 2177	18 28 47	−2 07 36

NOTE.—Where appropriate, an infrared source (IRS) is paired with its corresponding optical source (OS). Infrared source positions were measured at 2.3, 3.6, or 10 μm and with 5″ apertures. Optical source positions were measured on a print of the Palomar Observatory Sky Survey E series, a portion of which is reproduced in Fig. 1*f*. Positions (1b) referring to large-scale components of the W40 complex were measured with ~3′ apertures. Published 1 σ uncertainties are ~20″ for the position of peak H II emission (Goss and Shaver 1970) and ~2′ for AFGL 2177 (Price and Walker 1976). Positions of peak $^{12}CO(J = 1 \rightarrow 0)$ emission were taken from Zeilik and Lada 1978.

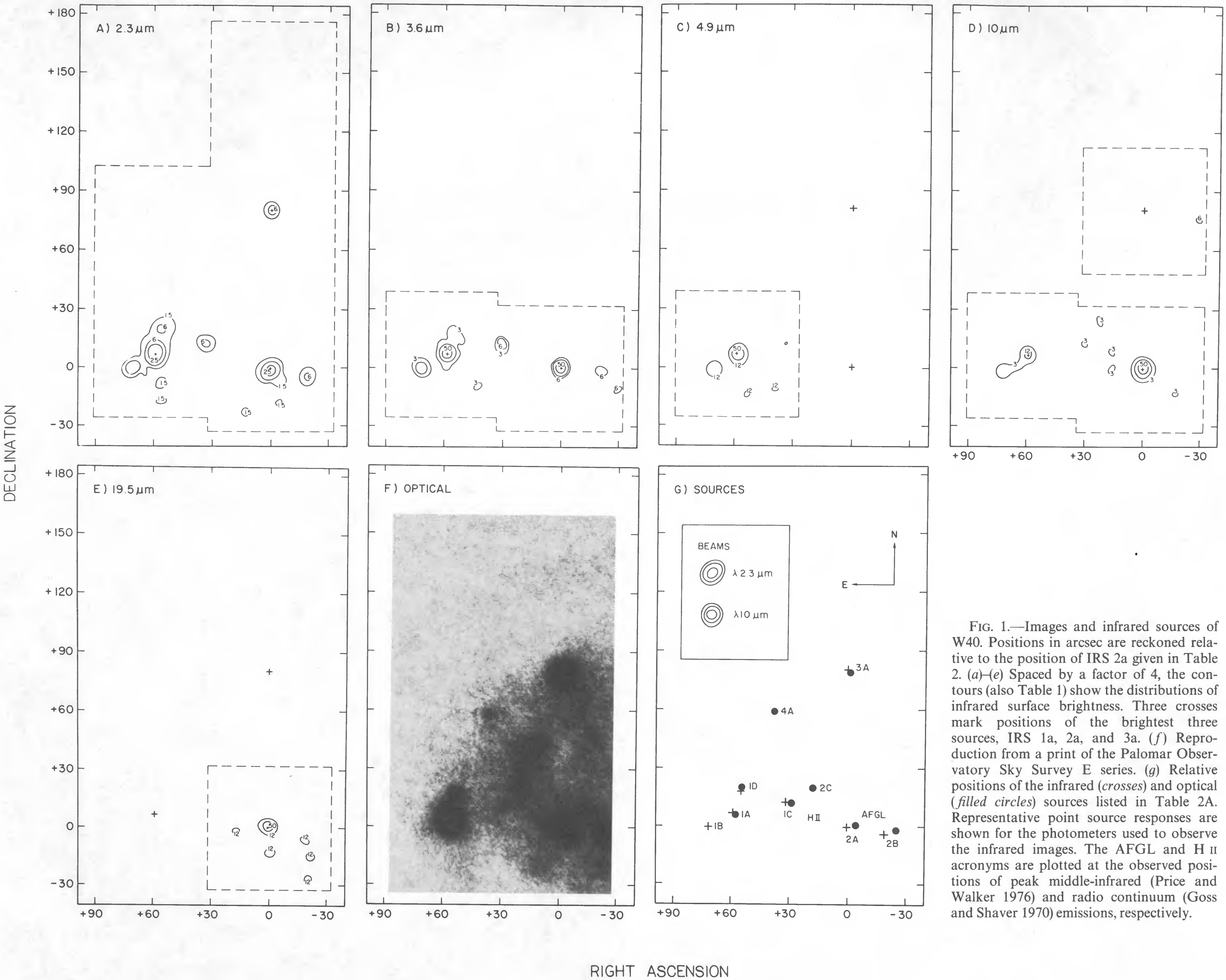

FIG. 1.—Images and infrared sources of W40. Positions in arcsec are reckoned relative to the position of IRS 2a given in Table 2. (*a*)–(*e*) Spaced by a factor of 4, the contours (also Table 1) show the distributions of infrared surface brightness. Three crosses mark positions of the brightest three sources, IRS 1a, 2a, and 3a. (*f*) Reproduction from a print of the Palomar Observatory Sky Survey E series. (*g*) Relative positions of the infrared (*crosses*) and optical (*filled circles*) sources listed in Table 2A. Representative point source responses are shown for the photometers used to observe the infrared images. The AFGL and H II acronyms are plotted at the observed positions of peak middle-infrared (Price and Walker 1976) and radio continuum (Goss and Shaver 1970) emissions, respectively.

TABLE 3

W40 PHOTOMETRY

Source	IRS 1a	IRS 1b	IRS 1c	IRS 2a	IRS 3a
$U-B$	0.6	...	...	1.1	0.9
$B-V$	2.2	...	...	2.7	2.4
V	15.0	...	...	16.1	15.6
$J-H$	1.3	...	...	1.6	0.9
$H-K$	1.0	...	...	0.9	0.5
$K-L$	1.3	2.0	1.1	1.7 ± 0.2	0.4
L	4.3	5.7	7.1	4.6	7.3
$L-M$	0.6	0.9	0.7	1.0	0.7
$L-[8.7\ \mu m]$	1.7	2.4	2.2	3.8	2.7 ± 0.2
$L-N$	1.8	2.7	2.4	4.5	3.2
$L-[11.4\ \mu m]$	2.2	3.1	2.6	5.0	3.4
$L-[12.6\ \mu m]$	2.3	2.9 ± 0.2	...	5.3	4.0 ± 0.2
$L-[19.5\ \mu m]$	3.2	4.7 ± 0.4	...	6.7	5.3 ± 0.4
$L-[23\ \mu m]$	...	...	...	7.5 ± 0.2	...

The shapes of the infrared energy distributions given in Figure 2 demonstrate that the three sources seen in the 10 μm images (IRS 1a, 1b, and 2a) have circumstellar emission. Flux densities of IRS 2a increase from 10 to 23 μm in a fashion expected of warm circumstellar dust. Infrared sources 1a and 1b show broad, roughly constant distributions of infrared flux density possibly from circumstellar material having a wide temperature range. Notice that photospheric radiation from a main-sequence star would have a monotonically decreasing flux density as the infrared wavelength increases.

Figure 2 presents evidence for circumstellar emission from two additional sources (IRS 1c, 3a) too faint to be imaged at 10 μm. At $\lambda \gtrsim 10$ μm, IRS 3a resembles IRS 2a, whereas IRS 1c has a broad infrared energy distribution much like that shown for IRS 1a. The small amount of information given in Figure 2b for IRS 1d and 2b was inferred from the 2.3 and 3.6 μm images of Figure 1.

From 3.6 to 12.6 μm, the energy distribution shapes (Fig. 2*b*) of IRS 1b and 1c resemble the approximately flat energy distribution of their nearest bright neighbor, IRS 1a. A noteworthy difference among the three energy distributions is the abrupt decrease occurring between 3.6 and 2.3 μm for IRS 1b, the only source of the three that has no visible companion on the POSS E print. Possible explanations of these two differences in IRS 1b are that it has a larger extinction or an intrinsically fainter star.

Zeilik and Lada (1978) give some energy distribution information for their sources, IRS 1, 2, and 3. Their data, observed with three different aperture sizes and a reference aperture spacing of 100″, can be compared with our detailed energy distributions of IRS 1a, 2a, and 3a, each observed with a 5″ aperture and a 60″ reference aperture spacing. Zeilik and Lada observed IRS 1 with an 18″ aperture. At K and L, their photometry of IRS 1 and our photometry of IRS 1a agree reasonably well. Beyond 3.6 μm, the photometry of IRS 1 and IRS 1a differ: the energy distribution of IRS 1 increases strongly from 5 to 20 μm in a fashion expected of warm dust, whereas IRS 1a shows a broad and nearly flat energy distribution. The energy distributions given by Zeilik and Lada for IRS 2 and 3 cover the small wavelength ranges of 1.65–5.0 and 1.25–5.0 μm, respectively. Observed through a 16″ aperture, their photometry of IRS 2 agrees reasonably well with our photometry of IRS 2a. In contrast, their photometry of IRS 3, observed through a large 46″ aperture, differs from our photometry of IRS 3a: IRS 3 is fainter at J and H but brighter at the larger K and L wavelengths. In summary, the photometric observations reported by Zeilik and Lada are brighter than or equal to our values at K and longer wavelengths; at the shorter J and H wavelengths, their data are equal to or fainter than ours.

The way in which the WIRO and Zeilik and Lada energy distributions depend on aperture size and reference aperture spacing suggests that W40 has extended distributions of infrared emission. Some good evidence for extended emission from interstellar dust is the large ratio of IRS 1/IRS 1a flux densities

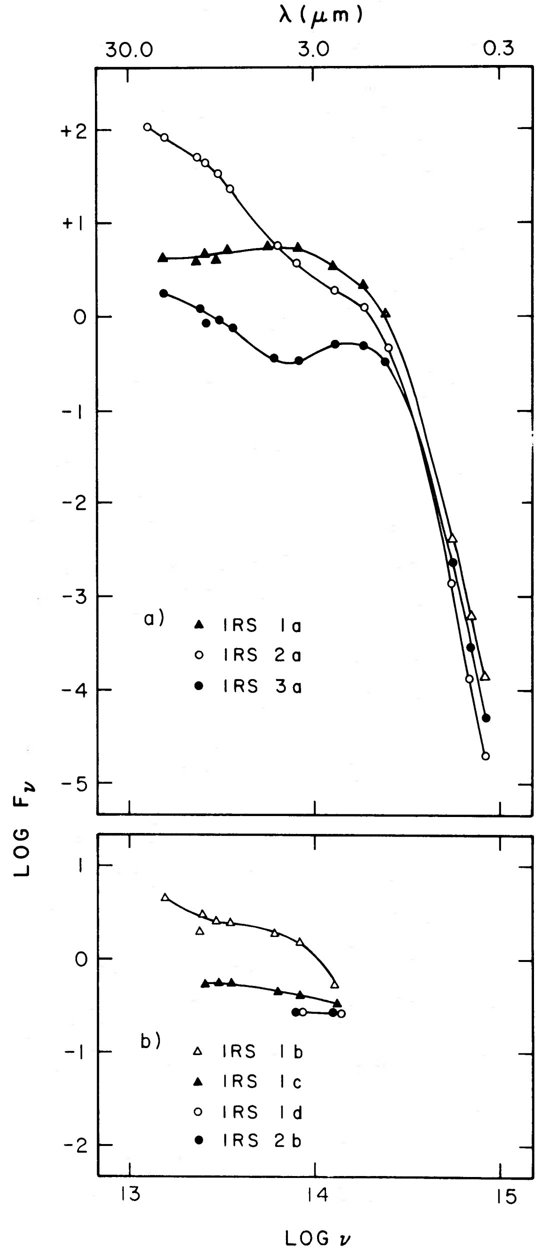

FIG. 2.—Energy distributions of the seven infrared sources observed in W40. Logarithm of flux density (F_ν in Jy) is plotted against logarithm of radiation frequency. Solid lines show smooth trends in the data plotted for each source. See Table 3 for the broad-band photometry plotted for IRS 1a, 1b, 1c, 2a, and 3a. Flux densities of IRS 1d and 2b were inferred from the infrared images shown in Figs. 1a and 1b. (*a*) Optical through infrared energy distributions of IRS 1a, 2a, and 3a. (*b*) Infrared energy distributions of IRS 1b, 1c, 1d, and 2b. The upper limit plotted at 3.6 μm for IRS 2b is 3 σ.

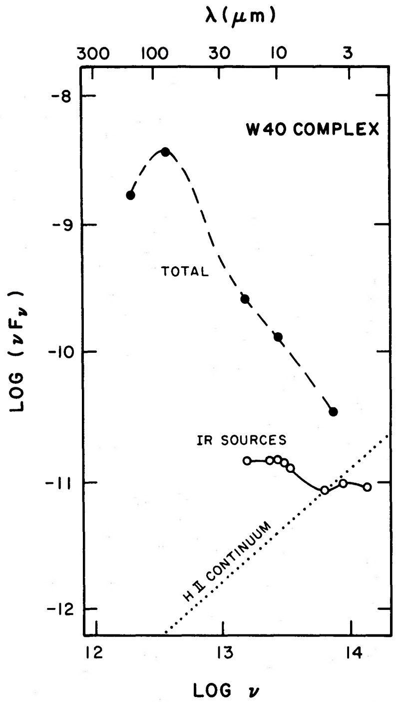

FIG. 3.—Infrared energy distributions of the W40 complex. Logarithm of the product of frequency times flux density (νF_ν in W m^{-2}) is plotted against logarithm of the frequency. Extending from 2.3 to 19.5 μm, the solid line shows the nearly flat spectral distribution of the sum (*open circles*) of the flux densities measured for the five brightest infrared sources and given individually in Table 3. Connected by the dashed line, filled circles show the 4, 11, and 20 μm measurements made by Price and Walker (1976) with a 3$'$.5 × 10$'$.5 aperture and the 83 and 155 μm measurements made by Oltof (1974) with a 30$'$ aperture. The monotonically increasing dotted line is an unextinguished extrapolation of the 1.4–5.0 GHz H II emissions measured by Altenhoff *et al.* (1970) with an 11$'$ aperture.

amounting to a factor of ~10 in the 10–20 μm interval. In addition, photometric errors may contribute to the large difference between observations of IRS 1 and 1a. The differences observed between IRS 3 and IRS 3a may require extended emissions of two types: emission from hot interstellar dust may explain the differences observed at *K* and *L*, whereas photospheric emission produced by the widely distributed infrared cluster of W40 (Smith 1984) may explain the differences observed at the shorter *J* and *H* wavelengths.

The presentation of Figure 3 reveals some additional information concerning the origin of infrared emissions observed in W40. Total flux densities were inferred from the large beam measurements of Price and Walker (1976) and Olthof (1974) made at middle-infrared and far-infrared wavelengths, respectively. The contribution of compact infrared sources to each total flux density is approximated by the sum of the flux densities measured for IRS 1a, 1b, 1c, 2a, and 3a (Table 3); using the low-resolution observations of IRS 1, 2, and 3 made by Zeilik and Lada (1978) would make no qualitative difference in our discussion. For observed wavelengths of the 10–20 μm interval, the combined emission of the five infrared sources accounts for <10% of the total emission. This small contribution of the infrared sources and also the shape of the W40 energy distribution suggest that diffuse clouds of dust having a wide temperature range produce almost all the middle-infrared and far-infrared emissions observed for W40. About 96% of the total W40 emission is produced beyond 20 μm, suggesting that the cool component of the diffuse dust is the predominant source of reradiation in W40. Much of the 4% remainder emitted short of 20 μm appears to be produced by a warm component of the diffuse dust possibly closely associated with the H II plasma. Near 4 μm, the total emission must be produced by a complex combination of sources including the infrared sources and the H II gas, each of which contributes ~25% of the total amount.

Before the levels of excitation can be estimated for the diffuse clouds of dust and H II gas in W40, their distance must be specified. The distance adopted for our work is 700 pc (Goss and Shaver 1970). This value was inferred from recombination line observations of the W40 H II region and the kinematic model of the Galaxy. Another datum that tends to confirm this relatively small distance of W40 is its galactic latitude of 3°.5. This latitude requires that W40 be no more distant than ~800 pc if it is to reside within the ~100 pc thick plane normally populated by the Galaxy's H II regions.

The level of dust cloud excitation may be inferred from the infrared observations given for the W40 complex in Figure. 3. Summing the fluxes implied by the dashed curve gives 5×10^{-9} W m^{-2} for the 4–200 μm flux of the W40 complex. That flux, or its equivalent luminosity of 7.5×10^4 $L_\odot$, could originate from dust heated by a single O9 V star. This same O9 V level of excitation can be calculated for the H II gas from radio observations. For the H II region of W40, Altenhoff *et al.* (1969) give 35 Jy for the radio continuum emission and Pankonin, Thomassohn, and Barsuhn (1977) give $He^+/H^+ = 0.09$ for the 166α ratio of recombination line fluxes. Both the Lyman-continuum luminosity of $\sim 1.5 \times 10^{48}$ photon s^{-1} inferred from the continuum emission and the approximate excitation temperature implied by the recombination ratio could be produced by a single O9 V star.

IV. DISCUSSION

a) Energy Distributions of the Compact Sources

The evaluation of accurate monochromatic extinctions is a crucial part of any attempt to decompose an observed energy distribution into circumstellar and photospheric components. Table 4 gives results of the sequence of steps leading to the monochromatic extinctions of W40-IRS 3a. First, we found that the IRS 3a photometry of the 0.55–4.9 μm interval could be explained by the photospheric emission of a B1 V star lying at the W40 distance of 700 pc and obscured by a standard type of interstellar extinction (Savage and Mathis 1979). As a result, the $E(V-\lambda)$ excess colors were computed as the observed colors (the $V-[\lambda]$) minus the intrinsic colors of a B1 V star

TABLE 4

MONOCHROMATIC EXTINCTIONS OF W40-IRS 3a

λ(μm)	$V-[\lambda]$ (mag)	$E(V-\lambda)$ (mag)	A_v (mag)	A_λ (mag)
0.36.........	−3.3	−4.5	...	14.5
0.44.........	−2.4	−2.7	...	12.7
0.55.........	...	...	...	10.0
1.25.........	6.7	7.3	10.1	2.8
1.65.........	7.6	8.3	10.2	1.9
2.3	8.0	8.8	9.9	1.2
3.6	8.3	9.2	9.8	0.6
4.9	9.0	9.9	10.1	0.2
10.0	11.1	12.1	...	0.0
Mean............			10.0	

(Johnson 1966). Using the five excess colors of the 0.55–4.9 μm interval and standard interstellar values of $A_v/E(V-\lambda)$, we computed 10.0 mag for the mean visual extinction of IRS 3a. The last step of the extinction analysis was to use the derived 10.0 mag of visual extinction to compute each of the values of monochromatic extinction (A_λ). For $\lambda \geq 0.55$ μm, each value of A_λ was computed as the product of the 10.0 mag and the appropriate standard value of A_λ/A_v. For the shorter B and U wavelengths, the monochromatic extinctions were computed directly from the excess colors as $10.0 + E(B-V)$ and $10.0 + E(U-V)$. Values of $A_v/E(B-V)$ and $A_v/E(U-V)$ implied by this analysis are 3.8 and 2.2, respectively. Differing little from the standard values of 3.1 and 1.9, those extinction ratios emphasize the predominantly standard nature of the monochromatic extinctions affecting the observed energy distribution of IRS 3a.

Figure 4 shows the energy distribution of W40-IRS 3a decomposed into photospheric and circumstellar components. The photospheric energy distribution is normalized to the V flux density of IRS 3a and has the shape determined by the intrinsic colors of a B1 V star modified by the monochromatic extinctions of Table 4. The circumstellar energy distribution of IRS 3a, derived by subtracting the photospheric flux densities from the observed values, is indicative of warm circumstellar dust at ~270 K. The circumstellar luminosity of the 5–20 μm interval is ~4 $L_\odot$ or ~0.01% of the total luminosity of a B1 V star.

Unlike the colors of IRS 3a, the colors of IRS 1a and 2a do not show convincing evidence for predominantly photospheric emission extending from optical to near-infrared wavelengths. Therefore, we must seek an alternative to the method of inferring a mean value of visual extinction from the observed optical-infrared colors. A reasonable alternative is to use the IRS 3a ratios of $A_v/E(B-V)$ and $A_v/E(U-V)$ together with values of the excess colors, $E(B-V)$ and $E(U-V)$. For each star, the excess colors were computed from the observed colors

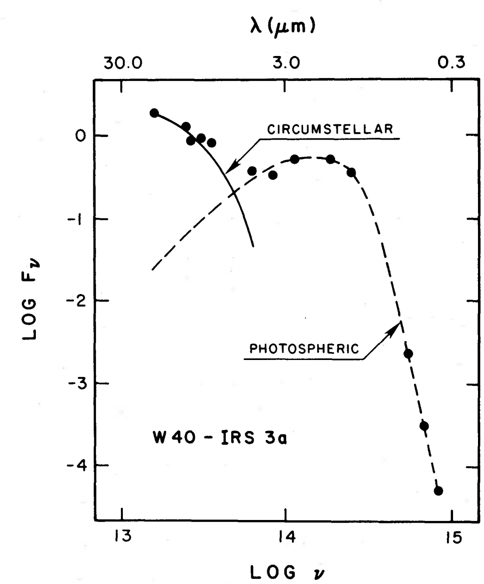

FIG. 4.—Decomposition of the W40-IRS 3a energy distribution into circumstellar and photospheric components. Observed data are plotted as filled circles. Data observed for the 0.55–4.9 μm interval are fitted to the photospheric emission of a B1 V photosphere (*dashed line*) obscured by interstellar dust producing $A_v = 10$ mag. Shown connected by the solid line, the circumstellar flux densities are the observed minus the photospheric flux densities.

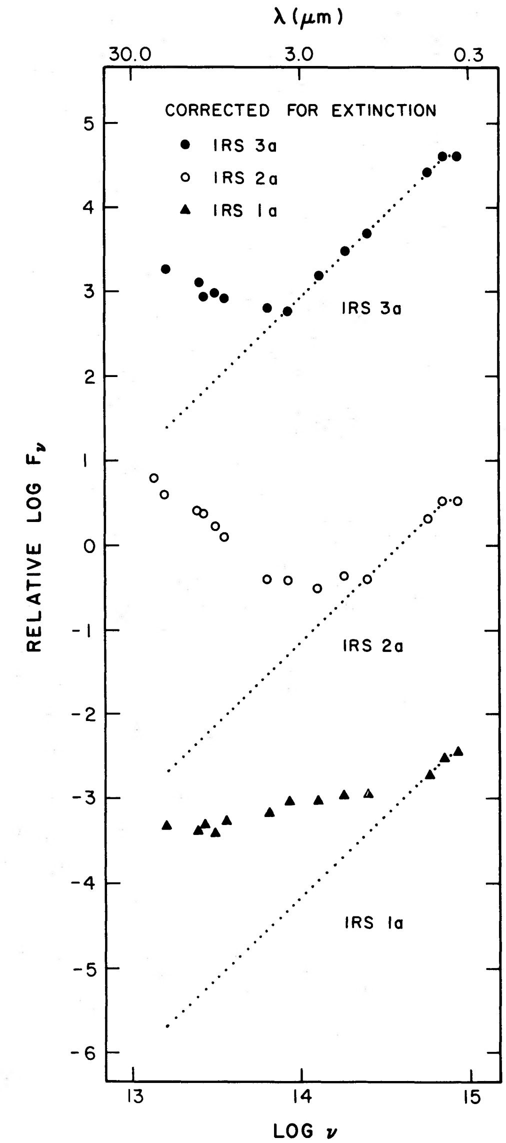

FIG. 5.—Energy distributions of W40 sources corrected for interstellar extinction. Each dotted line shows the shape of a B1 V energy distribution normalized to the corrected V flux density. A display constant (C) added to the logarithm of flux density (F_ν in Jy) is plotted against logarithm of radiation frequency. Values of C are +3, −4/3, and −4 for IRS 3a, 2a, and 1a, respectively.

(Table 3) and B1 V as a noncritical approximation to the spectral type. Values of mean visual extinction inferred by this alternative method are 9.2 and 11.3 mag for IRS 1a and 2a, respectively. Monochromatic extinctions are inferred from each of these values of visual extinction in the same way described above for IRS 3a.

Figure 5 shows the energy distributions of IRS 1a, 2a, and also 3a corrected for the interstellar extinctions computed above. Also plotted in Figure 5 are the energy distributions of a B1 V photosphere normalized to the corrected visual flux density of each star. Although circumstellar emission becomes important for IRS 3a only at wavelengths longer than 4.9 μm, it dominates the energy distributions of IRS 1a and 2a at much shorter wavelengths.

It proves informative to compare the W40 sources with other objects which have been studied in some detail. Figure 6*a*

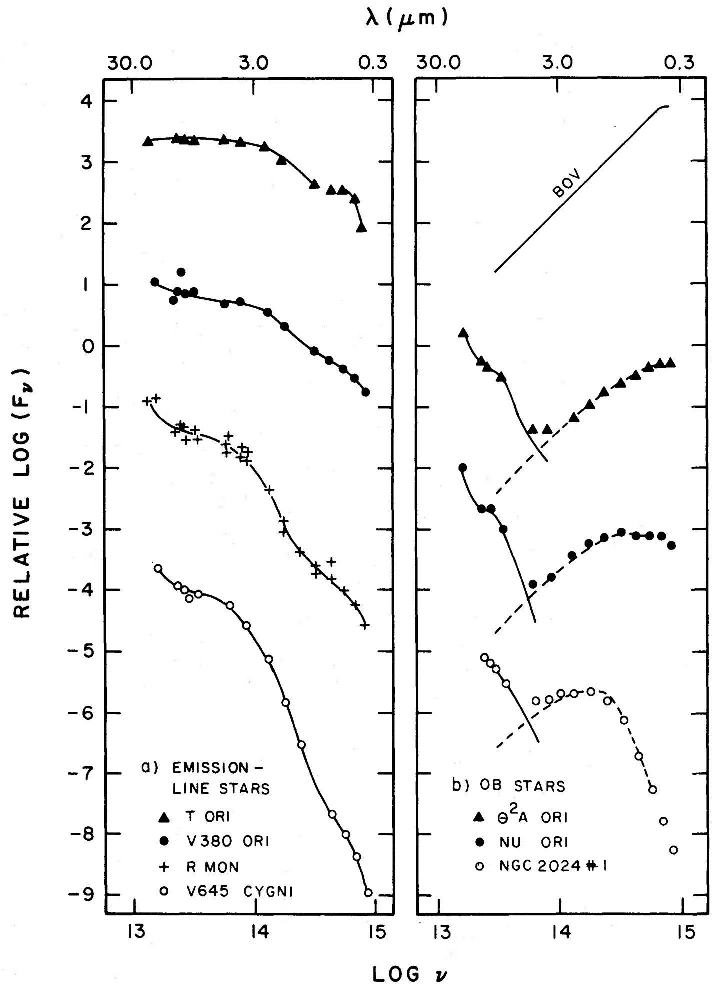

FIG. 6.—Energy distributions of comparison stars used to study the observed W40 sources. For each star of the two panels, a display constant (C) added to the logarithm of flux density (F_ν in Jy) is plotted versus the logarithm of observed radiation frequency. (*a*) A sequence of hot, emission-line stars ordered according to their 10.0/0.55 μm ratio of flux densities. Similar to W40-IRS 1a, 1b, and 1c, $F_\nu \approx$ constant for substantial positions of the infrared energy distributions. Solid curves show merely trends in the flux densities. Values of C are +3, 0, −3, and −6 for T Ori (B8–A3pe), V380 Ori (B8–A2e), R Mon (−e +shell), and V645 Cygni (A5e), respectively. References for the plotted flux densities are Walker (1969), Penston (1973), and Smith (1976) for T Ori; Lee (1970), Low *et al.* (1970), Cohen (1973), and Allen (1973), for V380 Ori and R Mon; and Humphreys, Merrill, and Black (1980) for V645 Cygni. References for the emission-line spectra are Johnson (1965) for T Ori; Herbig (1959, 1962) for V380 Ori, and R Mon; Humphreys *et al.* for V645 Cygni. (*b*) Extinction sequence of comparison OB stars related to W40-IRS 3a. Symbols show the observed flux densities. Photospheric flux densities (*dashed lines*) were computed from intrinsic stellar colors modified by interstellar extinction. Connected by a solid line for each star, circumstellar flux densities are the observed minus the photospheric flux densities. Values of (A_v, C) are (0, 0), (1.1, −2.0), (2.2, −4.0), and (7.8 mag, −6.0) for the intrinsic energy distribution of a B0 V star (top, $V = 0$ mag), θ^2A Ori (O9.5 V), NU Ori (B0.5 V), and NGC 2024 No. 1 (bottom, B0.5 V), respectively.

shows the energy distributions of four comparison stars, T Ori, V380 Ori, R Mon, and V645 Cygni, each of which is a hot emission-line star associated with nebulosity. Like W40-IRS 1a, 1b, and 1c, the emission-line stars tend to have $F_\nu \approx$ constant for a substantial portion of their 2–20 μm energy distributions. Thus, IRS 1a, 1b, and 1c may be hot emission-line stars. Figure 6*b* shows the energy distributions of three additional comparison stars, θ^2A Ori, NU Ori, and NGC 2024 No. 1, each of which is a relatively normal OB star with a reradiating circumstellar dust cloud. Like W40-IRS 3a, each of these OB stars has a circumstellar energy distribution that increases strongly from 5 to 20 μm. Thus, the case is strengthened for IRS 3a being a main-sequence OB star surrounded by a cloud of reradiating dust grains. Figure 5 shows that W40-IRS 2a has characteristics of both the emission-line and main-sequence OB stars: for the 1–5 μm interval, the corrected flux densities of IRS 2a are nearly constant, whereas, for wavelengths longer than 5 μm, the energy distribution of IRS 2a increases strongly like those of the main-sequence OB stars.

The summary presented in Table 5 includes descriptions of W40-IRS 3a and the three comparison stars, θ^2A Ori, NU Ori, and NGC 2024 No. 1. The above analysis of IRS 3a gives the guidelines used to derive monochromatic extinctions for each of the comparison stars. For each of IRS 3a, θ^2A Ori, NU Ori, and NGC 2024 No. 1, the value of $L_c/L_{\rm IR}$ shows that circumstellar emission (L_c) is a substantial portion of the total infrared emission ($L_{\rm IR}$). However, relative to the photospheric emission (L_p) estimated for each star, the value of L_c is small. Thus, very little of each star's luminosity is reradiated by circumstellar dust at 5–20 μm.

Because the photospheric components are very difficult to identify for IRS 1a and 2a, the summaries presented in Table 5 for these two stars are relatively uncertain. Nevertheless, these summaries should be useful for purposes of comparison. Each

TABLE 5

PROPERTIES OF SELECTED SOURCES

Source	Sp	A_v (mag)	$\frac{A_v}{E(B-V)}$	$\frac{A_v}{E(U-V)}$	V_0 (mag)	M_v (mag)	T_c (K)	T_B (K)	L_{IR} ($L_\odot$)	L_c ($L_\odot$)	$\frac{L_c}{L_{IR}}$ (percent)	$\frac{L_c}{L_p}$ (percent)
A. Compact W40 Sources												
IRS 1a	(OB)	9	(3.8)	(2.2)	5.8	−3.5	350	79	90	(80)	(90)	(0.3)
IRS 1b	...	...	...	...	...	...	280	77	30	...	...	...
IRS 1c	...	...	...	...	...	...	...	71	>7	...	...	...
IRS 2a	(OB)	11	(3.8)	(2.2)	4.9	−4.3	250	89	230	(220)	(90)	(0.3)
IRS 3a	(OB)	10	3.8	2.2	5.5	−3.7	270	73	10	4	40	(0.01)
B. Embedded OB Stars												
θ^2A Ori	09.5V	1.1	4.7	2.8	4.0	−4.0	200	...	100	90	80	0.1
NU Ori	B0.5V	2.2	4.1	2.4	4.6	−3.4	170	...	50	40	80	0.2
NGC 2024 No. 1	B0.5V	7.8	4.6	2.6	4.4	−3.6	...	...	>13	>5	>40	>0.02

NOTE.—The optical and infrared photometric data used in calculating the entries were taken from Table 3 for the sources of W40; from Lee 1968, Iriarte *et al.* 1965, Penston 1973, and Ney, Strecker, and Gehrz 1973 for θ^2A Ori and NU Ori; and from Johnson 1968 and Grasdalen 1974 for NGC 2024 No. 1. A specific OB spectral type of B1 V was adopted in analyses of the W40 sources; depending on future spectral classification work, values enclosed within parentheses may be revised. Iriarte *et al.* 1965, Schild and Chaffee 1971, and Johnson and Mendoza 1974 give the spectral types for θ^2A Ori, Nu Ori, and NGC 2024 No. 1, respectively. The text describes how the values of visual extinction (A_v) were computed. Intrinsic visual magnitudes are given by $V_0 = V - A_v$. Distance moduli (DM) used in computing the absolute visual magnitudes ($M_v = V_0 - \mathrm{DM}$) and luminosities (L_{IR}, L_c, L_p) are 9.2 and 8.0 mag for the W40 and other sources, respectively. Blackbody color temperatures (T_c) are computed from the 10/20 μm ratio of flux densities. Each blackbody brightness temperature (T_B) refers to the source's 10 μm surface brightness averaged over the $\sim$20 arcsec^2 aperture. Values of L_{IR} are total amounts of infrared luminosity produced in the 2.3–20 μm wavelength interval. Values of L_c are the circumstellar portions of the values of L_{IR}. Photospheric luminosities (L_p) were computed from the values of M_v and bolometric corrections (Code *et al.* 1976) implied by the spectral types.

of the three sources, IRS 1a, 2a, and 3a, consists of a heavily obscured OB star associated with a compact circumstellar source. This interpretation differs in two basic ways from the view developed by Zeilik and Lada (1978) for their low-resolution observations of W40. They described their three brightest sources not as being compact but as resolved, $\sim$30″ diameter regions of diffuse emission. Second, they argued that extinction by dust should not affect substantially the W40 energy distributions, whereas our analysis implies substantial values of $\sim$10 mag for the visual extinctions.

b) Morphology and Energetics

Basic elements of the W40 morphology (Fig. 7) include: (1) the brightest and therefore probably densest portion of the extensive molecular complex observed by Zeilik and Lada (1978), (2) the large, $\sim$5′ diameter H II region (Goss and Shaver 1970; Altenhoff *et al.* 1970) lying in a side-by-side and possibly contiguous relationship with the bright molecular core, and (3) the seven detected infrared sources distributed within a 1′.5 diameter region centered approximately on the position of peak H II emission.

The close association of the infrared sources with the H II region, the absolute visual magnitudes (M_v) summarized in Table 5, and the level of excitation derived for both the dust and H II gas (§ III) suggest that some combination of the brightest detected sources (IRS 1a, 2a, 3a) has enough luminosity to ionize the H II gas and heat much of the dust of the W40 complex. IRS 2a appears to be the most luminous star; we suggest that it is the most important single source of excitation.

Estimates of extinction optical depths constrain the possible modes whereby the observed sources heat the dust distributed throughout the W40 complex. To compute extinction optical depths for the dust, we assume that the dust extinctions obey a standard interstellar curve (Savage and Mathis 1979) and that optical reddening is related to the nucleon column density according to the standard interstellar relation given by Bohlin, Savage, and Drake (1978). These two assumptions lead to $A_{uv} \approx 1 \times 10^{-21} N_H$ mag, the desired relation between the ultraviolet extinction (A_{uv}) and the nucleon column density (N_H). Using this relation, we estimate ultraviolet extinctions of $\lesssim$3 and $\sim$30 mag for the columns of dust associated with the H II and molecular gases, respectively. For the H II region, N_H

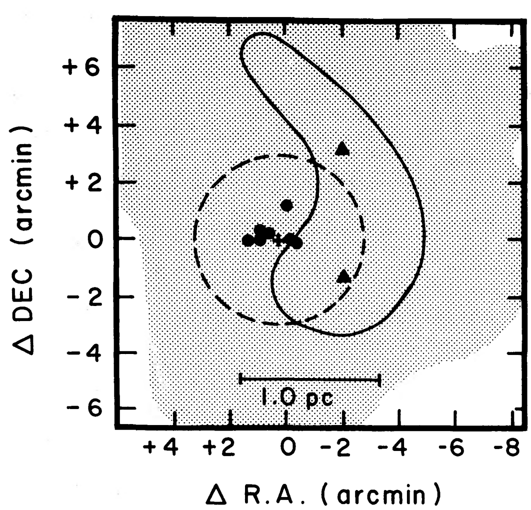

FIG. 7.—Elements of the W40 morphology. Shading shows where emission from the CO molecule has been detected in the 14′ × 14′ region covered by the figure. The solid line encloses the bright molecular core for which the peak brightness temperatures of CO ($J = 1 \rightarrow 0$) emission are in the 15–31 K range. The positions of peak CO emission are plotted as filled triangles. Centered at the cross plotted $\sim$2′.5 northwest of the position of brightest CO emission, the 5′ diameter H II region (*dashed line*) lies side by side with the molecular core. Filled circles show positions of the seven detected infrared sources all of which lie near the position of peak H II emission. Positions in arc minutes are reckoned relative to the IRS 2a position plotted as (0, 0). At the adopted distance of 700 pc, the scale is 1′ = 0.20 pc.

was equated to the $\sim 1 \times 10^{21}$ cm^{-2} electron column density (Shaver and Goss 1970); A_{uv} is an upper limit because dust that would ordinarily be associated with the $\sim 1 \times 10^{21}$ cm^{-2} column density of nucleons may be modified or expelled by the harsh ultraviolet radiation field of the H II region. For the molecular complex, wherein $N_H = 2N_{H_2}$ applies, we computed a peak value of N_H from $N_{H_2} = 5 \times 10^5 N_{13}$ (Dickman 1978) and $N_{13} = 5 \times 10^{16}$ cm^{-2}, the ^{13}CO column density given by Zeilik and Lada (1978) for the position of Peak 1 (Table 1). Using the relative distribution of ^{12}CO($J = 1 \rightarrow 0$) emission (Zeilik and Lada 1978) to scale the peak column density gives $N_H \approx 3 \times 10^{22}$ cm^{-2} for molecules distributed along the lines of sight intercepting the embedded infrared sources.

Now that we have proposed the major sources of excitation and estimated some extinction optical depths for the volume of W40, we can proceed to discuss some general aspects of the dust cloud energetics. A small portion of the total amount of diffuse dust, surrounding the cluster and having $A_{uv} \approx 1$, could absorb and then reradiate much of the cluster's luminosity. Depending on whether dust is depleted in the H II region and also on the accuracy of the above extinction calculation, much of this dust with $A_{uv} \approx 1$ may reside within an interface between the H II boundary and molecular cloud. This leaves a large amount of cooler dust, mixed with the molecules and isolated by significant ultraviolet extinction from the energetic sources of the H II region, to be heated by radiation from a complex combination of sources including the obscured exciting stars, additional members of the widely distributed W40 star cluster (Smith 1984), and the warm dust grains near the H II region. Each of the two dust components will contribute to the total reradiation spectrum of the W40 complex, but the small amount of diffuse dust irradiated directly by the exciting stars will contribute most to the far-infrared reradiation.

A small amount of diffuse dust may lie within the circumstellar region of each of the infrared stars. Although this hypothetical component would have a negligible impact on the energetics of W40, we can show that its presence could account for a significant portion of the circumstellar emissions observed for IRS 2a and 3a. We can estimate the size of a cloud of diffuse dust for which $L_c/L_p < 0.01$, a limit to the levels given for the 5–20 μm reradiations of IRS 2a and 3a (Table 5). Along its diameter, the cloud would produce $A_{uv} \approx 2L_c/L_p$ for the extinction at ultraviolet wavelengths or $<1\%$ of the ~ 3 mag estimated for the assumed unmodified dust mixed with the plasma. If 5′, roughly the observed width of the H II region, approximates the distance to which the 3 mag refers, then the diffuse cloud would be $<2''$ in diameter. In addition to this compact size, we would expect the circumstellar component of the diffuse dust to have a 10/20 μm color temperature larger than the ~ 200 K inferred from the AFGL measurements made with a large beam (Fig. 3). Both expected properties of the diffuse circumstellar emission are consistent with the observations: the images show that IRS 2a is compact at both 10 and 20 μm and the sets of photometry give ~ 250 K for the 10/20 μm color temperatures of IRS 2a and 3a.

The differences in shape observed for the infrared energy distributions of IRS 1a, 2a, and 3a suggest some intrinsic differences among their circumstellar regions. Harvey, Thronson, and Gatley (1979) have discussed how the shape of a circumstellar energy distribution may depend on the density profile of the circumstellar material. One of their models suggests that strongly increasing energy distributions of the type observed at $\lambda \geq 10$ μm for IRS 2a and 3a are produced by circumstellar dust grains having a uniform density. Within the context of this model, our above discussion implies that the uniformly distributed dust surrounding IRS 2a and 3a may be a small portion of the diffuse interstellar medium of W40. A second model considered by Harvey, Thronson, and Gatley (1979) suggests that broad energy distributions of the type observed for the emission-line stars V380 Ori and R Mon (also Fig. 6*a*) are produced by circumstellar condensations of dust. W40-IRS 1a, and possibly IRS 1b and 1c, have broad energy distributions resembling those of the emission-line stars and therefore are candidates for circumstellar condensations.

Being clustered tightly within a small, ~ 0.2 pc diameter region of the W40 complex, the seven W40 sources may have approximately the same epoch of formation. If so, these objects would have roughly the same age yet they have a diverse set of properties. For example, IRS 1a has the $F \approx$ constant type of circumstellar spectrum, whereas IRS 3a has circumstellar emission that increases strongly beyond ~ 5 μm. Perhaps this diversity of form results from the way that a compact object evolves within its H II region and molecular cloud complex. In the case of W40, the evolution appears to depend in a complex way on the individual evolutions not only of the embedded star and any circumstellar condensation it may have, but also the star's diffuse environment.

V. SUMMARY

We have presented observations revealing a cluster of seven compact infrared sources in W40, all but one of which can be associated with optically identified stars. Being heavily obscured and centered on the H II region, the three brightest sources (IRS 1a, 2a, 3a) are reasonable candidates for producing the level of excitation observed for both the dust and the H II plasma. The circumstellar regions observed for the brightest five sources (IRS 1a, 1b, 1c, 2a, 3a) have little impact on the overall energetics of the W40 dust. Instead, the most important mode of excitation appears to involve the diffuse clouds of dust. The infrared energy distributions exhibit a wide range of shapes, suggesting intrinsic differences among the distributions of circumstellar material.

We thank H. Chisolm and R. Shaw for their work with the detection systems and operations of the telescope. J. Gasaway and M. Lee typed the manuscript. Infrared Astronomy at the Wyoming Infrared Observatory is supported by the NSF, the US Air Force, and the State of Wyoming.

REFERENCES

Allen, D. A. 1973, *M.N.R.A.S.*, **161**, 145.
Altenhoff, W. J., Downes, D., Goad, L., Maxwell, A., and Rinehart, R. 1970, *Astr. Ap. Suppl.*, **1**, 319.
Bohlin, R. C., Savage, B. D., and Drake, J. F. 1978, *Ap. J.*, **224**, 132.
Code, A. D., Davis, J., Bless, R. C., and Hanbury Brown, R. 1976, *Ap. J.*, **203**, 417.
Cohen, M. 1973, *M.N.R.A.S.*, **161**, 105.
Dickman, R. 1978, *Ap. J. Suppl.*, **37**, 407.
Gehrz, R. D., Grasdalen, G. L., Castelaz, M., Gullixson, C., Mozurkewich, D., and Hackwell, J. A. 1982, *Ap. J.*, **254**, 550 (Paper II).
Gehrz, R. D., Hackwell, J. A., and Jones, T. W. 1974, *Ap. J.*, **191**, 675.
Goss, W. M., and Shaver, P. A. 1970. *Australian J. Phys. Ap. Suppl.*, No. 14, p. 1.

Hackwell, J. A., Grasdalen, G. L., and Gehrz, R. D. 1982, *Ap. J.*, **252**, 250 (Paper I).
Harvey, P. M., Thronson, H. A., and Gatley, I. 1979, *Ap. J.*, **231**, 45.
Herbig, G. H. 1959, *Ap. J. Suppl.*, **4**, 337.
———. 1962, *Adv. Astr. Ap.*, **2**, 1.
Humphreys, R. M., Merril, K. M., and Black, J. H. 1980, *Ap. J.* (*Letters*), **237**, L17.
Iriarte, B., Johnson, H. L., Mitchell, R. I., and Wiśniewski, W. K. 1965, *Sky and Tel.*, **30**, 21.
Johnson, H. L. 1966, *Ann. Rev. Astr. Ap.*, **4**, 193.
Johnson, H. L., and Mendoza, E. E. 1964, *Bol. Obs. Tonantzintla y Tacubaya*, **3**, 331.
Johnson, H. L., Mitchell, R. I., Iriarte, B., and Wiśniewski, W. Z. 1966, *Comm. Lunar Planet. Lab.*, No. 63.
Johnson, H. M. 1965, *Ap. J.*, **142**, 964.
Lee, T. A. 1968, *Ap. J.*, **152**, 913.
Lee, T. J. 1970, *Pub. A.S.P.*, **82**, 765.
Low, F. J., Johnson, H. L., Kleinmann, D. E., Latham, A. S., and Geisel, S. L. 1970, *Ap. J.*, **160**, 531.
Ney, E. P., Strecker, D. W., and Gehrz, R. D. 1973, *Ap. J.*, **180**, 809.
Olthof, H. 1974, *Astr. Ap.*, **33**, 471.
Pankonin, V., Thomasson, P., and Barsuhn, J. 1977, *Astr. Ap.*, **54**, 335.
Penston, M. V. 1973, *Ap. J.*, **183**, 505.
Price, S. D., and Walker, S. G. 1976, *AFGL Four Color Infrared Sky Survey* (Environmental Research Papers No. 576).
Savage, B. D., and Mathis, J. S. 1979, *Ann. Rev. Astr. Ap.*, **17**, 73.
Schild, R. E., and Chaffee, F. 1971, *Ap. J.*, **169**, 529.
Smith, J. 1976, Ph.D. thesis, University of Wyoming.
———. 1984, private communication.
Walker, M. F. 1969, *Ap. J.*, **155**, 447.
Zeilik, M., and Lada, C. J. 1978, *Ap. J.*, **222**, 896.

A. Bentley, M. Castelaz, R. D. Gehrz, G. L. Grasdalen, J. A. Hackwell, and J. Smith: Department of Physics and Astronomy, The University of Wyoming, University Station, Box 3905, Laramie, WY 82071